JBC RESEARCH ARTICLE

Nudix hydrolase 18 catalyzes the hydrolysis of active triphosphate metabolites of the antivirals remdesivir, ribavirin, and molnupiravir

Received for publication, March 22, 2022, and in revised form, June 15, 2022 Published, Papers in Press, June 19, 2022,
https://doi.org/10.1016/j.jbc.2022.102169

Ann-Sofie Jemth[1,*], Emma Rose Scaletti[2], Evert Homan[1], Pål Stenmark[2], Thomas Helleday[1,3], and Maurice Michel[1,*]

From the [1]Science for Life Laboratory, Department of Oncology-Pathology, Karolinska Institutet, Solna, Sweden; [2]Department of Biochemistry & Biophysics, Stockholm University, Stockholm, Sweden; [3]Weston Park Cancer Centre, Department of Oncology & Metabolism, Medical School, University of Sheffield, Sheffield, United Kingdom

Edited by Patrick Sung

Remdesivir and molnupiravir have gained considerable interest because of their demonstrated activity against SARS-CoV-2. These antivirals are converted intracellularly to their active triphosphate forms remdesivir-TP and molnupiravir-TP. Cellular hydrolysis of these active metabolites would consequently decrease the efficiency of these drugs; however, whether endogenous enzymes that can catalyze this hydrolysis exist is unknown. Here, we tested remdesivir-TP as a substrate against a panel of human hydrolases and found that only Nudix hydrolase (NUDT) 18 catalyzed the hydrolysis of remdesivir-TP with notable activity. The k_{cat}/K_m value of NUDT18 for remdesivir-TP was determined to be 17,700 $s^{-1}M^{-1}$, suggesting that NUDT18-catalyzed hydrolysis of remdesivir-TP may occur in cells. Moreover, we demonstrate that the triphosphates of the antivirals ribavirin and molnupiravir are also hydrolyzed by NUDT18, albeit with lower efficiency than Remdesivir-TP. Low activity was also observed with the triphosphate forms of sofosbuvir and aciclovir. This is the first report showing that NUDT18 hydrolyzes triphosphates of nucleoside analogs of exogenous origin, suggesting that NUDT18 can act as a cellular sanitizer of modified nucleotides and may influence the antiviral efficacy of remdesivir, molnupiravir, and ribavirin. As NUDT18 is expressed in respiratory epithelial cells, it may limit the antiviral efficacy of remdesivir and molnupiravir against SARS-CoV-2 replication by decreasing the intracellular concentration of their active metabolites at their intended site of action.

The recent SARS-CoV-2 pandemic with its fast worldwide spread and high mortality rate led to put major efforts to repurpose already approved antiviral drugs in order to quickly control the outbreak and thereby save lives. Remdesivir (GS-5734) was originally developed for the treatment of Ebola but is a broad-acting antiviral which has been found to reduce the replication of coronaviruses both in cell culture and animal models (1). Remdesivir treatment was shown to decrease the severity of disease after MERS-CoV infection via decreasing virus replication and thereby reducing damage to the lungs when administered both before and after infection in a rhesus macaque model (1). Recently, remdesivir was tested in several clinical trials for treatment of COVID-19 caused by the coronavirus SARS-CoV-2. Remdesivir was shown to shorten the recovery time of hospitalized adults with COVID-19 as well as reducing the mortality rate (2) and suggested to be most effective if administered early after infection (3). Remdesivir was the first drug to be approved for the treatment of severe COVID-19 in July 2020 by the European Medicines Agency and later in the fall by the U.S Food and Drug Administration (2, 4–6). Remdesivir is a prodrug in the form of a protected phosphate that upon cell entry (Fig. 1, step 1) is metabolized by cellular enzymes to the corresponding monophosphate (GS-441524, Fig. 1, step 2). The monophosphate is subsequently phosphorylated by cellular kinases to its active triphosphate form (remdesivir-TP, aka GS-443902, Fig. 1, step 3). The antiviral effect of remdesivir-TP is mediated through its incorporation into the growing virus RNA chain by the viral RNA-dependent RNA polymerase (Fig. 1, step 4). Incorporation of the remdesivir metabolite causes the polymerase to stall and RNA replication to be terminated (Fig. 1, step 5), leading to a decrease in the production of viral RNA (7, 8).

Molnupiravir (EIDD-2801) was, in November 2021, given a temporary authorization by the UK's Medicines and Healthcare products Regulatory Agency for the treatment of mild to moderate COVID-19 in adults at risk for severe disease and one month later, an emergency use authorization was issued by the Food and Drug Administration agency. Administration of this orally active drug led to a clear reduction of SARS-CoV-2 replication as well as a quicker recovery time (9). In addition, early treatment with molnupiravir clearly reduced the risk of death or hospitalization in unvaccinated adults with COVID-19 at risk for severe disease (10). Molnupiravir is a prodrug for β-d-N4-hydroxycytidine, which has previously been shown to be effective against various RNA viruses including influenza and other coronaviruses (11, 12) and is rapidly hydrolyzed to β-d-N4-hydroxycytidine followed by phosphorylation, resulting in formation of its active 5′ -triphosphate metabolite (13).

* For correspondence: Ann-Sofie Jemth, ann-sofie.jemth@ki.se; Maurice Michel, maurice.michel@ki.se.

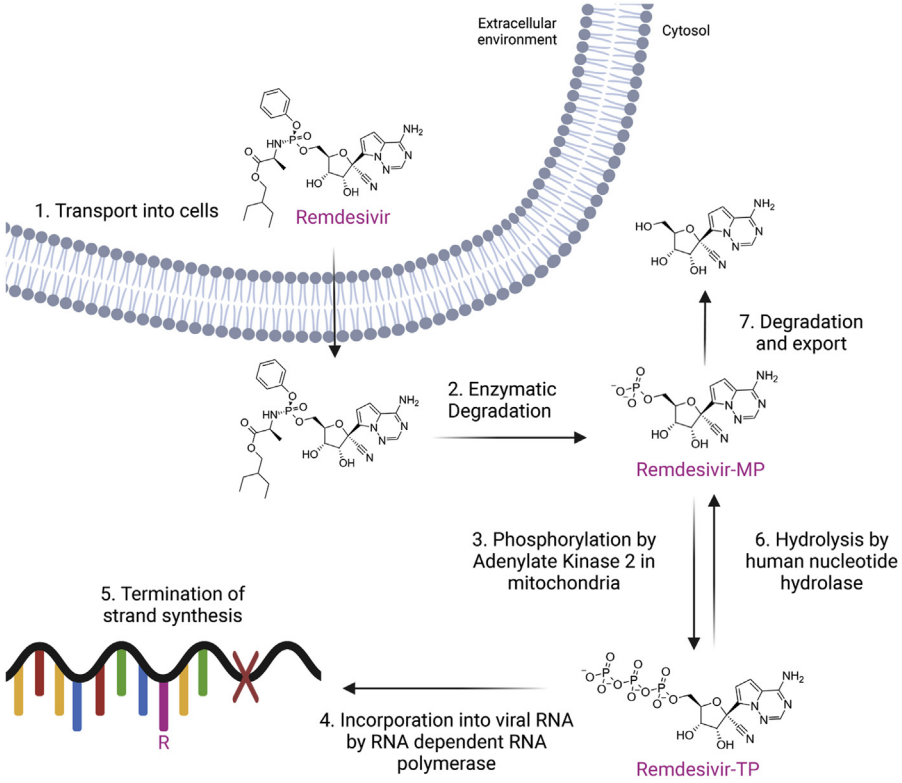

Figure 1. Structure, intracellular metabolism, and mode of action of remdesivir. Figure was created with BioRender.

The incorporation of β-d-N4-hydroxycytidine triphosphate, hereafter called molnupiravir-TP, by RNA-dependent RNA polymerase into viral RNA causes a drastic increase in the mutation frequency, resulting in a decrease in SARS-CoV-2 replication (14).

Ribavirin is another antiviral drug that was tested for activity towards SARS-CoV-2. Ribavirin has, since the 1970s, been known to act as a broad-spectrum antiviral for both DNA and RNA viruses (15). It has been used in combination with Interferon-α–based therapy to treat hepatitis C (16) as well as other viral infections such as Lassa fever (17), Crimean-Congo fever (18, 19) and chronic hepatitis E virus infections (20). Ribavirin in combination with Interferon-β was shown to synergistically inhibit SARS-associated coronavirus replication in animal and human cell lines (21), suggesting that ribavirin could be a potential treatment option for SARS-CoV-2. The precise mode of action of ribavirin is not completely understood and its metabolites have been suggested to target several processes, of which the antiviral impact may depend on their intracellular concentrations (22). However, it is known that ribavirin-MP inhibits inosine monophosphate dehydrogenase, leading to GTP depletion with effects on many cellular processes. Ribavirin-TP has been hypothesized to directly inhibit viral RNA-dependent polymerase and may at higher concentrations, also cause mutations in the viral genome. Ribavirin-TP is hydrolyzed by the inosine triphosphate pyrophosphatase (ITPase), and patients carrying alleles encoding low activity ITPase variants display a reduced risk of hepatitis C relapse, suggesting that these patients have higher concentrations of the active ribavirin metabolite. Furthermore, low activity ITPase alleles have been shown to protect against anemia acquired upon INF-α and ribavirin therapy (22, 23).

The ITPase activity–dependent outcome of ribavirin treatment strongly emphasizes the impact of cellular metabolism on drug efficacy. Similar to ITPase, several NUDIX enzymes catalyze the hydrolysis of modified nucleoside triphosphates (24, 25) and have been shown to modulate the efficacy of various drugs including antivirals (26, 27). An example is Nudix hydrolase (NUDT) 15, which we recently reported catalyzes the hydrolysis of ganciclovir-TP (27). In a similar way, hydrolysis of remdesivir-TP into remdesivir-MP, catalyzed by a human nucleotide hydrolase (Fig. 1, Step 6), would reduce the cellular concentration of the active metabolite. Moreover, conversion of remdesivir-MP to the corresponding nucleoside through the action of 5′-nucleotidase would enable its transport out of the cell (Fig. 1, Step 7) and further decrease the antiviral potency of remdesivir. In order to investigate if such a hydrolase could be found within the NUDIX family of enzymes, we tested remdesivir-TP as a substrate for a panel of human NUDIX hydrolases and found that NUDT18 catalyzed the hydrolysis of remdesivir-TP. Encouraged by this, we tested NUDT18 for activity toward several antiviral triphosphates and found NUDT18 to also be an efficient catalyst of ribavirin-TP and molnupiravir-TP hydrolysis. NUDT18 has, to date, only been described to display activity toward 8-oxo-dGDP and has therefore been suggested to cleanse the nucleotide pool from oxidatively damaged nucleotides, preventing their incorporation into DNA (28, 29). The results of this study

suggest that NUDT18 acts as a cellular sanitizer in a broader sense and contributes to removing modified nucleotides of both endogenous and exogenous origin and potentially modulates the efficiency of the antiviral drugs remdesivir, molnupiravir, and ribavirin.

Results and discussion

NUDT18 catalyzes the hydrolysis of remdesivir-TP and ribavirin-TP

In order to investigate if human NUDIX enzymes can modulate the cellular concentration of the active metabolite of remdesivir and thereby reduce its efficacy as an antiviral drug, we tested human MutT Homolog 1 (MTH1), NUDT5, NUDT9, NUDT15, and NUDT18 for hydrolysis activity with remdesivir-TP. This selection of NUDIX enzymes was chosen based on previous observations showing that MTH1, NUDT15, and NUDT18 have the capacity to hydrolyze nucleotide triphosphates or diphosphates (30). NUDT5 and NUDT9, which are the most closely related NUDIX enzymes to the NUDIX enzyme subgroup to which MTH1, NUDT15, and NUDT18 belong, catalyze the hydrolysis of nucleoside diphosphate sugars (30) and were added to the panel as NUDIX enzyme controls to assess NUDIX enzyme selectivity toward remdesivir-TP. Among these NUDIX hydrolases, only NUDT18 was found to catalyze the hydrolysis of remdesivir-TP (Fig. 2*A*). NUDT18 was shown to catalyze the hydrolysis of both the bonds between the α- and β-phosphate groups, generating PPi, as well as the bonds between the β- and γ-phosphate groups, generating Pi (Fig. 2, *A* and *B*). This was evidenced by an increase in the amount of Pi formed in the presence of pyrophosphatase (PPase), which hydrolyzes PPi. Of note, no general 5′-nucleotidase or PPase activity is present in the NUDT18 preparation used (30). Based on the described activity of ITPase with ribavirin-TP, which constitutes one of the active metabolites of the antiviral ribavirin, we argued that ITPase may also hydrolyze other antiviral triphosphates. We therefore tested human ITPase as well as the human hydrolases dCTPase and dUTPase for activity with remdesivir-TP. Human dCTPase displayed low but measurable activity with remdesivir-TP while no activity was detected with dUTPase or ITPase (Fig. 2*C*). Comparison with NUDT18 activity toward 8-oxo-dGDP showed an approximately 2-fold higher specific activity than remdesivir-TP at 100 μM substrate concentration (Fig. 2*C*).

The observed activity of NUDT18 with remdesivir-TP prompted us to test other antiviral triphosphates as substrates for NUDT18. We found that ribavirin-TP is also hydrolyzed by NUDT18, albeit not to the same extent as remdesivir-TP (Fig. 3*A*). Similar to remdesivir-TP, NUDT18-catalyzed ribavirin-TP hydrolysis results in the production of both ribavirin diphosphate and monophosphate, as shown by an increase in the signal when PPase was included in the assay buffer (Fig. 3*A*). NUDT18 was also shown to hydrolyze molnupiravir-TP. As evidenced by a 5-fold higher production of Pi in the presence of PPase (Fig. 3*B*), molnupiravir-TP hydrolysis of the bond between the α- and β-phosphate groups appears to be preferred. In addition, NUDT15, previously shown to catalyze the hydrolysis of ganciclovir-TP (27), was found to catalyze the hydrolysis of molnupiravir-TP producing pyrophosphate, albeit with considerably lower efficiency than NUDT18, while MTH1 did not display any detectable activity with this substrate (Fig. 3*B*). To investigate the activity of NUDT18 with these substrates in more detail and for comparison with 8-oxo-dGDP, we performed kinetic analyses of the NUDT18-catalyzed hydrolysis of remdesivir-TP, ribavirin-TP, and molnupiravir-TP. Enzyme activities were assayed under identical conditions and enzyme saturation curves using these substrates were produced (Fig. 4, *A–D*) and kinetic parameters were determined (Table 1). The K_m value for NUDT18 was determined to be 16.5 μM for 8-oxo-dGDP, which is in agreement with a previously published K_m value of

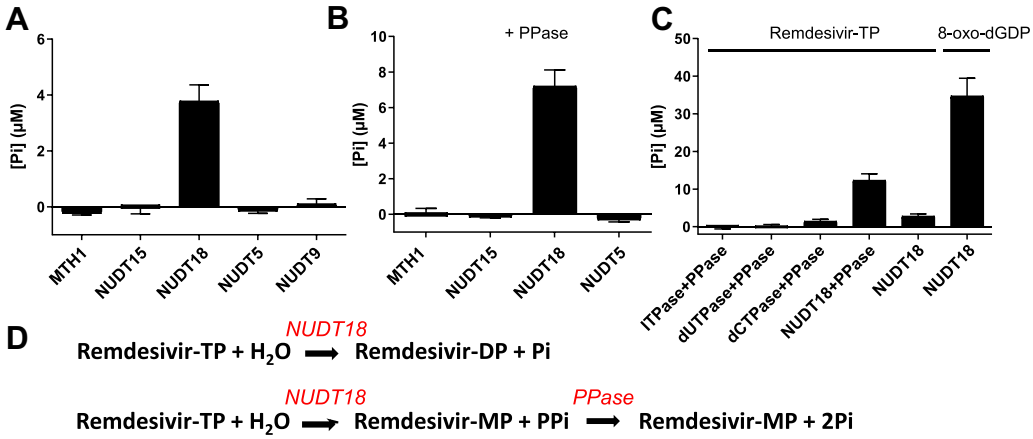

Figure 2. NUDT18 catalyzes the hydrolysis of remdesivir-TP. *A*, hydrolysis activity of MTH1, NUDT15, NUDT18, NUDT5, and NUDT9 (200 nM) with 100 μM remdesivir-TP was tested in assay buffer (20 mM Tris–acetate pH 8.0, 40 mM NaCl, 10 mM $Mg(Ac)_2$, 1 mM DTT, and 0.05% Tween20) by incubation at 22 °C for 30 min. Formed Pi was detected by addition of malachite green reagent and measurement of absorbance at 630 nm. *B*, activity of 200 nM MTH1, NUDT15, NUDT18, and NUDT5 was also tested in the presence of PPase (0.2 U/ml) that converts formed PPi to Pi. *C*, activity of the human pyrophosphatases ITPase, dUTPase, and dCTPase with 100 μM remdesivir-TP in the presence of PPase was assayed and compared to activity of NUDT18 with and without PPase and to NUDT18 activity with 100 μM 8-oxo-dGDP. *D*, hydrolysis products of NUDT18-catalyzed hydrolysis of remdesivir-TP in the presence and absence of NUDT18. Bars and error bars represent average and standard deviation determined from the mean of produced phosphate in two independent experiments in which phosphate production was assayed in duplicate. MTH1, MutT Homolog 1; NUDT, Nudix hydrolase; PPase, pyrophosphatase.

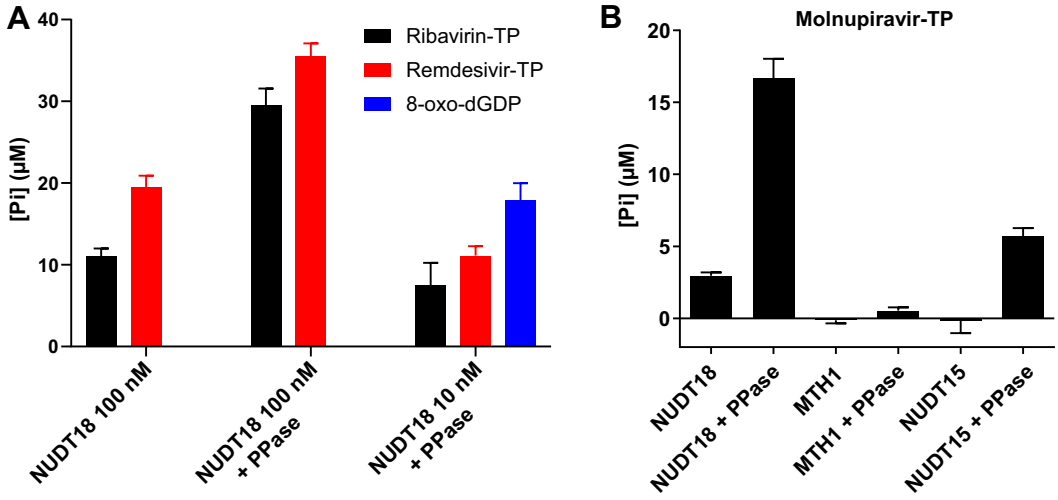

Figure 3. NUDT18 catalyzes the hydrolysis of ribavirin-TP and molnupiravir-TP. *A*, hydrolysis activity of 100 nM NUDT18 with 100 μM ribavirin-TP or remdesivir-TP, in the presence and absence of 0.2 U/ml *Escherichia coli* PPase, was monitored in assay buffer (20 mM Tris–acetate pH 8.0, 40 mM NaCl, 10 mM $Mg(Ac)_2$, 1 mM DTT, and 0.05% Tween20) by incubation at 22 °C for 30 min. Hydrolysis activity of 10 nM NUDT18 was assessed with 100 μM ribavirin-TP, remdesivir-TP, or 8-oxo-dGDP in assay buffer with *E. coli* PPase (0.2 U/ml) by incubating reactions at 22 °C for 30 min. *B*, hydrolysis activity of 20 nM NUDT18, MTH1, and NUDT15 was tested with 100 μM molnupiravir-TP, in the presence and absence of 0.2 U/ml *E coli* PPase by incubating reactions at 22 °C for 30 min. Formed Pi was detected by addition of malachite green reagent and measurement of absorbance at 630 nm. MTH1, MutT Homolog 1; NUDT, Nudix hydrolase; PPase, pyrophosphatase.

12 μM (28). The k_{cat} value for 8-oxo-dGDP at 22 °C was determined to be 1.8 s^{-1} and the calculated k_{cat}/K_m value was 109,800 $M^{-1}s^{-1}$. The K_m value for remdesivir-TP was determined to be 156 μM (n = 2) and the k_{cat} value was 2.6 s^{-1} resulting in a k_{cat}/K_m value of 17,700 $M^{-1}s^{-1}$. The approximately 6-fold higher catalytic efficiency (k_{cat}/K_m value) of NUDT18 for 8-oxo-dGDP means that 8-oxo-dGDP would be the preferred substrate over remdesivir-TP at the same concentration. However, the cellular remdesivir-TP concentration is likely in the order of 1000-fold higher than the concentration of 8-oxo-dGDP based on an estimation of the intracellular 8-oxo-dGTP concentration of 2 nM in U2OS cells (31), and the assumption that the cellular concentration of 8-oxo-dGDP is likely in a similar range or lower. This suggests that the

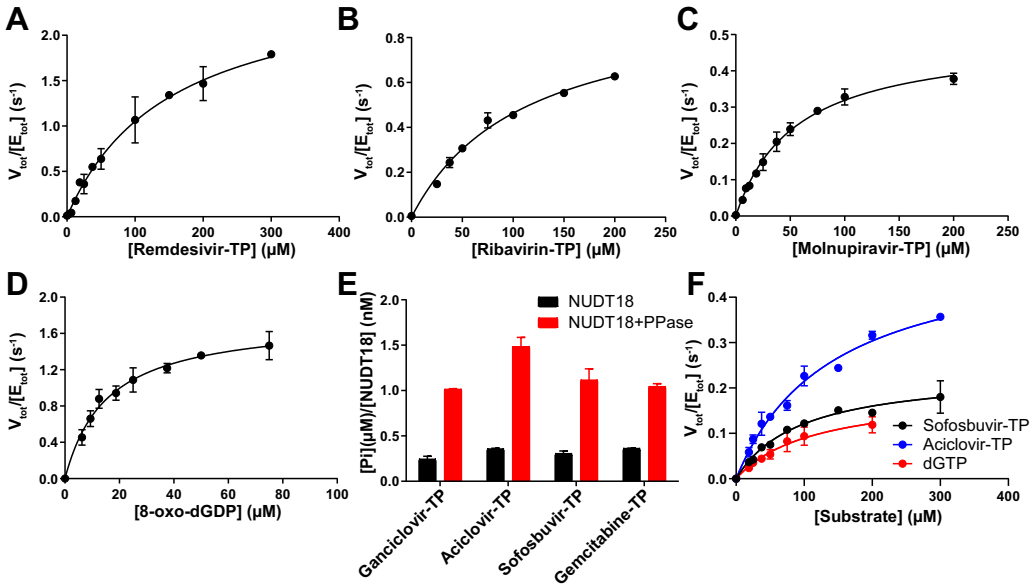

Figure 4. Kinetic analysis of NUDT18 with triphosphates of antiviral drugs. Enzyme saturation curves of NUDT18 with (*A*) remdesivir-TP, (*B*) ribavirin-TP, (*C*) molnupiravir-TP, and (*D*) 8-oxo-dGDP. *E*, specific activity of 20 nM NUDT18 with 100 μM of triphosphates of the antivirals ganciclovir, aciclovir, sofosbuvir, and the cytostatic drug gemcitabine was tested by incubation for 30 min at 22 °C in assay buffer (20 mM Tris–acetate pH 8.0, 40 mM NaCl, 10 mM MgAcetate, 1 mM DTT, and 0.01% Tween20), in the absence and presence of *Escherichia coli* PPase (0.2 U/ml). Formed Pi was detected using the addition of a malachite green reagent followed by measurement of absorbance at 630 nm. Figure shows formed [Pi] (μM) per [NUDT18] (nM). *F*, enzyme saturation curves of NUDT18 with sofosbuvir-TP, aciclovir-TP, and dGTP. Graphs with saturation curves show average and standard deviation of initial rates, determined from measurements of produced phosphate at 0, 10, 20, and 30 min performed in duplicate, from two independent experiments. MTH1, MutT Homolog 1; NUDT, Nudix hydrolase; PPase, pyrophosphatase.

Table 1
Kinetic parameters of NUDT18

Kinetic parameter	Substrate						
	dGTP	Sofosbuvir-TP	Aciclovir-TP	Remdesivir-TP	Molnupiravir-TP	Ribavirin-TP	8-oxo-dGDP
k_{cat} (s^{-1})	0.20 ± 0.07	0.24 ± 0.05	0.53 ± 0.01	2.6 ± 0.1	0.49 ± 0.01	0.98 ± 0.03	1.8 ± 0.2
K_m (μM)	117 ± 26	97 ± 22	146 ± 1.0	156 ± 60	57 ± 9	111 ± 5	16.5 ± 0.8
k_{cat}/K_m ($M^{-1}s^{-1}$)	1680 ± 190	2530 ± 70	3620 ± 90	17,700 ± 5800	8800 ± 1300	8810 ± 60	109,800 ± 6500

Presented is average and standard deviation of kinetic parameters determined from two independent experiments and with data points performed in duplicate.

activity of NUDT18 with remdesivir-TP may be of relevance for modulating the remdesivir-TP concentration in cells. The maximal plasma concentration of remdesivir in humans after treatment with a dose of 225 mg was reported to be around 7 μM and the concentration of remdesivir-TP in peripheral blood mononuclear cells was determined to be 6 μM after administration of 150 mg remdesivir (32, 33). The concentration of remdesivir-TP in cells seems to be higher than the remdesivir concentration in plasma, presumably due to the triphosphate formed in the cell not being cell membrane permeable. By applying the rule of thumb stating that an increase in temperature by 10 °C doubles the reaction rate, the catalytic efficiency of NUDT18 at 37 °C is estimated to be around 53,000 $M^{-1}s^{-1}$. Assuming a concentration of remdesivir-TP in the cell of 10 μM means that approximately one remdesivir triphosphate molecule will be turned over per NUDT18 enzyme every 2 sec, further supporting that remdesivir-TP is hydrolyzed by NUDT18 in the cell.

When comparing remdesivir-TP, ribavirin-TP, and molnupiravir-TP as substrates for NUDT18, remdesivir-TP appears to be the preferred substrate. NUDT18 displays a k_{cat} value for ribavirin-TP hydrolysis that is approximately 1 s^{-1} and a K_m value of 111 μM, resulting in a catalytic efficiency value of 8800 $s^{-1}M^{-1}$, which is approximately half of the corresponding value for remdesivir-TP (Table 1). The catalytic efficiency of NUDT18 for molnupiravir-TP was determined to 8800 $s^{-1}M^{-1}$, which is very close to the corresponding value for ribavirin-TP. However, both the K_m value (57 μM) and turnover number (0.49 s^{-1}) are approximately 2-fold lower for molnupiravir-TP. Comparison of the kinetic parameters of remdesivir-TP and ribavirin-TP with those of 8-oxo-dGDP shows that the difference primarily lies in the K_m value, suggesting a better fit of 8-oxo-dGDP in the active site of NUDT18.

NUDT18 catalyzes the hydrolysis of additional antiviral triphosphates

In order to investigate if NUDT18 can catalyze the hydrolysis of other antiviral triphosphates, we expanded the substrate screen of NUDT18 and found that sofosbuvir-TP, aciclovir-TP, ganciclovir-TP, as well as gemcitabine-TP are hydrolyzed by NUDT18 to some extent. Similar to the NUDT18-catalyzed hydrolysis of remdesivir-TP and ribavirin-TP, hydrolysis takes place at both the β–γ and the α–β phosphate bonds in these substrates with approximately 50% of the hydrolysis taking place at each of these positions (Fig. 4*E*). However, kinetic analysis revealed that the activity with aciclovir-TP, the best substrate in this panel, is much lower than the activity with remdesivir-TP, with a k_{cat}/K_m value approximately 5 times lower (Fig. 4, *F* and *G*). However, the k_{cat}/K_m value was 2.2 times higher than the corresponding k_{cat}/K_m value for dGTP. The fact that aciclovir contains a guanine moiety–like dGTP indicates that the higher activity of NUDT18 with aciclovir-TP than dGTP lies in NUDT18, being able to better accommodate the nucleobase and the modified sugar part of aciclovir-TP in the active site. This in turn enables a more productive positioning of the phosphate groups for hydrolysis. This is reflected by a 2.6 times higher turnover number (k_{cat}) for aciclovir-TP than that of dGTP, while the K_m values are comparable (Fig. 4*F*). However, whether the activity of NUDT18 with these antiviral triphosphates bears clinical relevance for modulating the potency of these antivirals needs further investigation.

Investigation of binding mode in NUDT18

Remdesivir-TP contains a nitrile group on the C1 atom of the ribose unit (Fig. 5). The fact that none of the other tested NUDIX proteins displays any activity with remdesivir-TP suggests that only the active site of NUDT18 is spacious enough and contains amino acids enabling accommodation of this moiety while still orienting the rest of the molecule allowing for efficient hydrolysis. To date, two crystal structures of human NUDT18 have been reported (Protein Data Bank (PDB) IDs: 3gg6 and 4hvy), both comprising apo structures of truncated constructs covering residue positions 26 to 179. Analysis of these structures using SiteMap (Schrödinger, Inc) indicated that the largest pocket adjacent to the helix containing the NUDIX motif is relatively small and polar in comparison to other NUDIX family members (34). Docking of remdesivir-TP to this site did not yield any good-scoring poses with plausible accommodation of the heterocyclic core of remdesivir-TP. In comparison, the homologous NUDIX family members NUDT1 and NUDT15 contain deeper druggable pockets which readily accommodate nucleobases and small-molecule inhibitors (35, 36). This suggests that considerable conformational changes are required for NUDT18 to harbor the heterocyclic cores of remdesivir-TP and other substrates. Attempts to induce a deeper hydrophobic pocket using an induced-fit procedure as described by Loving *et al.* (37) also failed to generate a pocket for remdesivir-TP with significantly improved SiteScore (Schrödinger).

In order to obtain structural information to understand the binding mode of NUDT18 substrates, we carried out extensive crystallization trials of full length NUDT18 without added ligands or together with 8-oxo-dGDP, remdesivir-TP, or

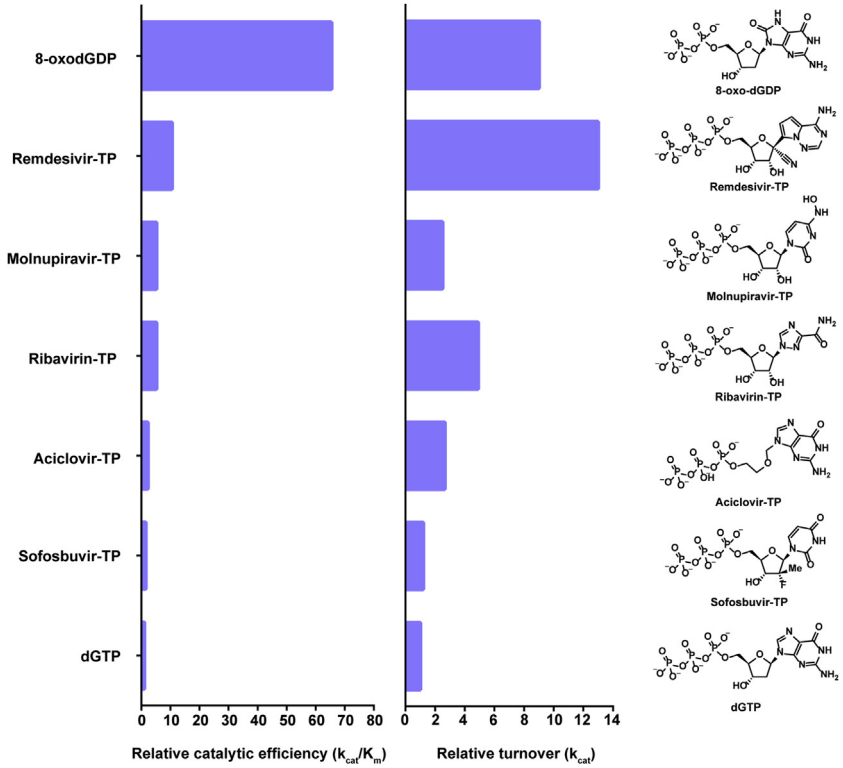

Figure 5. Relative catalytic efficiency and turnover numbers of NUDT18 with tested substrates and their chemical structures. NUDT, Nudix hydrolase.

ribavirin-TP. This included seven different commercially available crystallization screens (JCSG+, INDEX, Morpheus, Morpheus II, Pact Premier, Structure Screen, and Salt-RX) using different protein concentrations (ranging from 5 mg/ml to 25 mg/ml) and temperatures (4 °C and 20 °C). Unfortunately, we were not able to obtain crystals in any of the conditions tested. As only structures of the nucleosidase-binding domain are available for NUDT18, it is possible that the second domain and linking region render the full-length protein too flexible for crystallization. We performed a structural similarity search using the DALI web server (38), which indicated that hNUDT18 is most structurally similar to human and other eukaryotic MTH1 proteins from dogs, mice, and zebrafish (with rms differences of 2.1–2.3 Å). As remdesivir-TP is an analog of ATP, we were particularly interested in comparing the existing hNUDT18 nucleotidase domain structure (PDB ID: 3gg6) with structures of hMTH1 bound to N6-methyl-dAMP (PDB ID: 6qvo) (25) and 2-OH-dATP (PDB ID: 5ghq) (39). Comparison of these structures showed that residues from the highly conserved NUDIX motif (GX5EX7REVXEEXGU) that coordinate the essential magnesium ions required for substrate hydrolysis superimpose nicely between the structures (Fig. S1*A*). This provides some level of certainty as to where the α-phosphate group of remdesivir-TP would be positioned in hNUDT18 and therefore the orientation of the ligand within the binding pocket. Analysis of the hNUDT18 structure reveals a shallow binding pocket (Fig. S1*B*) and structural rearrangements are clearly required to accommodate the adenine base. Analysis of N6-methyl-dAMP and 2-OH-dATP binding in MTH1 shows that the residue W117* forms an important pi-stacking interaction with the adenine base. In NUDT18, the corresponding residue is an alanine; however, a tyrosine residue (Y72, N33* in hMTH1) which would be capable of performing an equivalent pi-stacking interaction is situated in close proximity (Fig. S1*C*). In the NUDT18 apo structure, Y72 clashes with the bound base when compared to the positioning of the ligands in the hMTH1 structures. A conformational adjustment must occur in order to make room for the substrate. Repositioning of this tyrosine would shape the binding pocket in such a way that it, while still being shallow, is capable of accommodating N6-methyl-dAMP and 2-OH-dATP and, importantly, remdesivir-TP with its additional nitrile group (Fig. S1*D*). The lower K_m value of 8-oxo-dGDP for NUDT18 suggests it fits better within the active site of the enzyme than remdesivir-TP. In the absence of a full-length NUDT18 structure, a structure of the NUDT18 nucleotidase domain bound to the natural substrate 8-oxo-dGDP or to remdesivir-TP would be very useful for elucidating the exact structural rearrangements that occur within the nucleotide binding site upon the binding of these ligands.

In an attempt to understand which structural features of the substrates that influence their quality as NUDT18 substrates, we compared their values of catalytic efficiency and turnover numbers of NUDT18-catalyzed hydrolysis for the tested substrates relative to the corresponding values for dGTP and examined the chemical structures of the tested substrates (Fig. 5). NUDT18 has previously been reported to catalyze the hydrolysis of 8-oxo-dGDP and 8-oxo-GDP with the same efficiency (28), demonstrating that the 2′-OH group can be

accommodated in the active site of NUDT18. This suggests a flexibility toward alterations within this part of the nucleoside substrate. Among the tested substrates, the turnover number is highest for remdesivir-TP, suggesting that either NUDT18-catalyzed hydrolysis or product release is faster for remdesivir-TP than 8-oxo-dGDP under substrate saturating conditions. However, the K_m value is considerably lower for 8-oxo-dGDP (Table 1), indicating specific interactions between the oxidized nucleobase and active site residues of NUDT18. The lower K_m value, which translates into higher catalytic efficiency for 8-oxo-dGDP, may in part be due to nucleoside triphosphates binding with lower affinity to the active site compared to nucleoside diphosphates. The difference in catalytic efficiency between remdesivir-TP and ribavirin-TP can likely be attributed to differences in positioning for efficient hydrolysis and/or product release since their K_m values are similar. The lower k_{cat} value for molnupiravir-TP than remdesivir-TP indicates a less efficient binding of molnupiravir-TP for productive catalysis. The NUDT18-catalyzed hydrolysis of molnupiravir-TP seems to take place mostly at the α–β phosphate bond while in the case of remdesivir-TP, hydrolysis occurs at both the β–γ and the α–β phosphate bonds to approximately the same extent (Fig. 3, *A* and *B*) suggesting that accommodation of the N4-hydroxycytidine moiety of molnupiravir-TP in the active site is more restricted in comparison to binding of the bicyclic triazin moiety of remdesivir-TP. Interactions between the nucleobase and/or the nitrile group of remdesivir-TP and NUDT18 may contribute to a more productive binding. However, in the absence of structural information, it is difficult to draw accurate conclusions about the binding mode. Nevertheless, the fact that the active site of NUDT18 can accommodate molecules with rather different structures and that hydrolysis takes place at two positions with equal efficiency, with the exception of molnupiravir-TP, indicates a relatively flexible binding mode for these substrates.

Inhibition of NUDIX enzymes by remdesivir and metabolites.

Since remdesivir-TP is a substrate for NUDT18, we argued that remdesivir and its metabolites may inhibit NUDT18 and related NUDIX proteins. We therefore tested MTH1 and NUDT15 for inhibition by remdesivir, the remdesivir metabolite GS-441524 (arising from cellular hydrolysis of remdesivir), and remdesivir-TP. We tested NUDT18 for inhibition by remdesivir and GS-441524. NUDT15 was found to be modestly inhibited by 100 μM remdesivir (26%) as well as by GS-441524 (21%) (Fig. 6). MTH1 was slightly inhibited by GS-441524 (23%) while no inhibition of NUDT18 by any of the tested remdesivir derivatives was observed. The modest inhibitory effect of remdesivir and its metabolites implies that remdesivir treatment is unlikely to have a pronounced effect on the cellular activity of these enzymes.

Consequence of NUDT18 activity with antiviral triphosphates

The results presented here suggest that NUDT18 can convert remdesivir-TP to remdesivir-DP and remdesivir-MP in the cell.

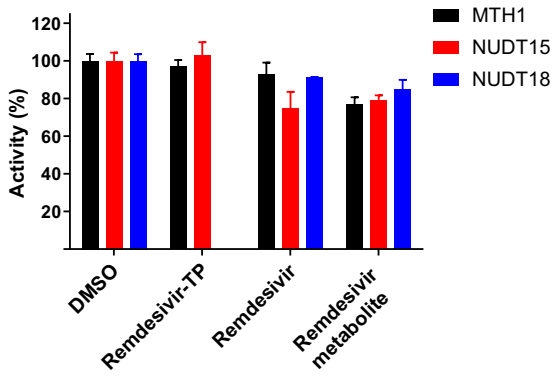

Figure 6. Inhibition of NUDIX enzymes by Remdesivir and its metabolites. MTH1 and NUDT15 was tested for inhibition by 100 μM remdesivir-TP, remdesivir, or remdesivir metabolite (GS-441524) in an activity assay using 100 μM dGTP as substrate and 10 nM NUDT15 or MTH1. The potency of remdesivir and remdesivir metabolite (GS-441524) to inhibit NUDT18 was tested in an assay using 100 μM 8-oxo-dGDP as substrate and using 100 nM NUDT18. NUDT15 is modestly inhibited by remdesivir, and activity of all three enzymes are reduced by approximately 20% in the presence of the remdesivir metabolite (GS-441524). MTH1, MutT Homolog 1; NUDT, Nudix hydrolase.

However, since remdesivir-DP and remdesivir-MP are substrates for adenylate kinase 2, they will be phosphorylated and a cellular equilibrium between the production of remdesivir-TP by kinases and hydrolysis catalyzed by NUDT18 is likely established. Furthermore, the action of intracellular 5′-nucleotidase will affect the concentration of remdesivir-MP. In a similar way, the cellular concentrations of the metabolites of molnupiravir and ribavirin will be regulated by the activities of adenylate kinase 2 and NUDT18 and in the case of Ribavirin and also ITPase. For NUDT18 to play a clinically relevant role in modulating remdesivir efficacy, it has to be present in the cells that are infected by the virus. Importantly, NUDT18 is ubiquitously expressed, displays low tissue specificity (https://www.proteinatlas.org/ENSG00000275074-NUDT18), and is expressed in the lungs and in respiratory epithelial cells (https://www.ebi.ac.uk/gxa/home). This suggests that NUDT18 would be able to modulate the effective concentration of remdesivir-TP and molnupiravir-TP at their intended site of action. Potentially, inhibition of NUDT18 would be a means to increase the efficacy of these drugs. However, no NUDT18 inhibitors enabling such investigations are available to the best of our knowledge.

The importance of intracellular metabolism for the efficiency of antivirals is exemplified by the activity of human ITPase with ribavirin-TP (22). Approximately, a third of the human population carries low activity ITPase alleles (22) and it is clear that cellular ITPase activity influences the antiviral efficacy of ribavirin as well as its adverse effects. Similarly, higher expression of NUDT18 in respiratory epithelial cells in a COVID-19 patient, potentially resulting in considerable remdesivir-TP and molnupiravir-TP hydrolysis, may result in lower efficiency of the corresponding antivirals than in a patient with lower NUDT18 expression levels. This may explain differences in response to remdesivir treatment between patients.

Here, we show that human NUDT18 can catalyze the hydrolysis of the active metabolites of the antivirals remdesivir,

ribavirin, and molnupiravir. These novel NUDT18 activities may be clinically relevant, warrant further investigation, and emphasizes the need for NUDT18-specific inhibitors, enabling studies of the cellular NUDT18 function and role in modulating the efficacy of these antiviral drugs.

In summary, we suggest a cellular role of NUDT18 as a sanitizer of modified nucleotides, including antiviral triphosphates.

Experimental procedures

Protein production

MTH1, NUDT15, NUDT18, NUDT5, NUDT9, and *Escherichia coli* PPase were produced as N-terminally His-tagged proteins and were expressed and purified by the Protein Science Facility, Karolinska Institute, using Ni-IMAC (HisTrap HP, GE Healthcare) followed by gel filtration (HiLoad 16/60 Superdex 75 or HiLoad 16/60 Superdex 100, GE Healthcare) as previously described (40). Proteins were concentrated and then stored as aliquots at −80 °C in storage buffer (20 mM Hepes pH 7.5, 300 mM NaCl, 10% glycerol, and 0.5 mM tris-(carboxyethyl)phosphine). ITPase, dUTPase, and dCTPase were produced as N-terminally His-tagged proteins and expressed and purified as earlier described (35).

Screen of human hydrolases for remdesivir-TP activity

Hydrolysis activity of MTH1, NUDT15, NUDT18, NUDT5, and NUDT9 (200 nM) with 100 μM remdesivir-TP was assayed in reaction buffer (20 mM Tris–acetate pH 8.0, 40 mM NaCl, 10 mM $Mg(Ac)_2$, 1 mM DTT, 0.01% Tween20) by incubating reaction mix in wells of clear 96-well plates (Nunc 269620) at 22 °C for 30 min. Formed Pi was detected by addition of malachite green reagent (41) and measurement of absorbance at 630 nm. Activities of 200 nM MTH1, NUDT15, NUDT18, and NUDT5, with 100 μM remdesivir-TP were also tested in the presence of *E. coli* PPase (0.2 U/ml), which converts formed PPi to Pi. Activity of the human PPases: ITPase, dUTPase, and dCTPase with 100 μM remdesivir-TP in the presence of PPase (0.2 U/ml) was assayed and compared to activity of NUDT18 with 100 μM 8-oxo-dGDP. Buffer controls with and without PPase were included, and the background signal was subtracted from the assay data.

Assessment of specific activity of NUDT18 with remdesivir-TP, ribavirin-TP, and 8-oxo-dGDP

In order to test if NUDT18 can also hydrolyze ribavirin-TP and to compare its activity toward remdesivir-TP (Biosynth Carbosynth) and 8-oxo-dGDP (Jena Bioscience), 100 μM Ribavirin-TP (Jena Bioscience), Remdesivir-TP, or 8-oxo-dGDP, respectively, was incubated with 10 nM NUDT18 in reaction buffer (20 mM Tris–acetate pH 8.0, 40 mM NaCl, 10 mM $Mg(Ac)_2$, 1 mM DTT, and 0.01% Tween20) fortified with 0.2 U/ml PPase for 30 min at 22 °C after which formed Pi was detected by the addition of malachite green reagent and measurement of absorbance at 630 nm in a Hidex spectrophotometer.

Assessment of specific activity with molnupiravir-TP

In order to test the activity of NUDT18 with the active metabolite of the orally active antiviral molnupiravir, molnupiravir-TP, and to investigate if the closely related NUDIX enzymes NUDT15 and MTH1 can hydrolyze this substrate hydrolysis activity of 20 nM NUDT18, MTH1 and NUDT15 was tested with 100 μM molnupiravir-TP, in the presence and absence of 0.2 U/ml *E. coli* PPase. Reactions were incubated at 22 °C for 30 min and the formed Pi was detected by addition of malachite green reagent with the measurement of absorbance at 630 nm.

Determination of kinetic parameters of NUDT18 with remdesivir-TP, ribavirin-TP, and molnupiravir-TP

Initial rates of NUDT18 (10 nM) were determined in assay buffer (20 mM Tris–acetate pH 8.0, 40 mM NaCl, 10 mM $Mg(Ac)_2$, 1 mM DTT, 0.01% Tween20, 0.2 U/ml PPase) at concentrations ranging from 0 to 300 μM for remdesivir-TP and from 0 to 200 μM for ribavirin-TP and molnupiravir-TP. Reaction mixtures were incubated for 0, 10, 20, and 30 min. Formed Pi was detected by adding malachite green reagent and measurement of absorbance at 630 nm. A Pi standard curve was included on the plate and used to convert absorbance to Pi concentration. Enzyme saturation curves were also produced with 8-oxo-dGDP, which has been described to be the endogenous substrate of NUDT18, using the same enzyme concentration and buffer conditions. 8-oxo-dGDP concentrations ranging between 0 and 100 μM were used. Initial rates were calculated using linear regression and plotted against substrate concentration. The Michaelis–Menten equation was fitted to the data points and kinetic parameters of NUDT18 were determined using GraphPad Prism 8.0. Initial rates were calculated from data points assayed in duplicate at each substrate concentration, and two independent experiments were performed.

Assessment of specific activity of NUDT18 with triphosphates of other antivirals

The finding that NUDT18 displays pronounced activity with the antiviral triphosphates remdesivir-TP, ribavirin-TP and molnupiravir-TP prompted us to also test the activity of NUDT18 with an expanded panel of antiviral triphosphates that are considered to be the active antiviral metabolite. The panel included the triphosphates of the following: sofosbuvir used for the treatment of hepatitis C (sofosbuvir-TP, (2R)-(2′-deoxy-2′-fluoro-2-methyl-uridine-5′-TP), Sierra bioresearch), ganciclovir used to treat cytomegalovirus infection treatment (ganciclovir-TP, Sierra bioresearch), and aciclovir used for Herpes simplex virus infection therapy, (aciclovir-TP, Sierra bioresearch). We also included the active metabolite of the cytostatic drug gemcitabine (gemcitabine-TP, Sierra bioresearch). NUDT18 (20 nM) was incubated with 100 μM of ganciclovir-TP, aciclovir-TP, sofosbuvir-TP, and gemcitabine-TP for 30 min at 22 °C in assay buffer (20 mM Tris–acetate pH 8.0, 40 mM NaCl, 10 mM $Mg(Ac)_2$, 1 mM DTT, and 0.01% Tween20), in the presence and absence of PPase 0.2 U/ml.

Formed Pi was detected by addition of malachite green reagent followed by measurement of absorbance at 630 nm.

Determination of kinetic parameters of NUDT18 with triphosphates of antiviral compounds

Initial rates of NUDT18 (10 nM) were determined in assay buffer (20 mM Tris-acetate pH 8.0, 40 mM NaCl, 10 mM $Mg(Ac)_2$, 1 mM DTT, 0.01% Tween20, and 0.2 U/ml PPase) at concentrations ranging from 0 to 300 μM for sofosbuvir-TP and aciclovir-TP by incubating the reactions for 0, 10, 20, and 30 min. Formed Pi was detected by adding malachite green reagent and measurement of absorbance at 630 nm. The concentration of formed Pi was calculated using a Pi standard curve included on the assay plate. Enzyme saturation curves were also produced for dGTP (GE Healthcare #27-1870-04) using a concentration range between 0 and 200 μM. Initial rates were plotted against substrate concentration and the Michaelis–Menten equation was fitted to the data points, allowing kinetic parameters of NUDT18 to be determined. Data points were measured in duplicate and two independent experiments were performed.

Computational analysis

All calculations were performed using Schrödinger Suite 2021-1 (https://www.schrodinger.com/releases/release-2021-2). *Protein structure preparation.* The apo structure of human NUDT18 (3GG6.pdb, unpublished) was prepared using the Protein Preparation Wizard. Briefly, the raw PDB structure was processed by automatically assigning bond orders, adding hydrogens, converting seleno-methionine to methionine, adding missing side chains, and creating possible disulfide bridges. Residues with alternate positions were locked in the conformations with the highest average occupancy. Hydrogen bonding networks were optimized automatically by optimization of hydroxyls, Asn, Gln, and His residue states using ProtAssign. A restrained minimization was then performed using the OPLS4 force field, until an RMSD convergence of 0.30 Å was reached for the heavy atoms.

Binding site analysis

SiteMap was used to probe the prepared NUDT18 structure for possible ligand-binding sites. The five top-ranked potential binding sites were identified. At least 15 site points per reported sites were required. A more restricted definition of hydrophobicity together with a standard grid (0.7 Å) were used. Site maps at 4 Å or more from the nearest site points were cropped.

Ligand structure preparation

The structure of remdesivir-TP was copied as isomeric smiles from PubChem (CID: 56832906) and pasted as a 3D structure into Maestro. Ligprep was then used to prepare the structure of remdesivir-TP for docking. The OPLS4 force field was used for minimizations; possible ionization states at pH 7.0 ± 2.0 were generated using Epik and possible tautomers were generated; specified chiralities were retained and at most one stereoisomer was generated.

Induced-fit docking

Remdesivir-TP was docked to NUDT18 using the induced-fit docking protocol (42). The site points of largest site identified by SiteMap were used to center the docking boxes. The size of the enclosing box was set to 20 Å. Glide XP was used for the redocking step, otherwise all settings were kept at default values.

Inhibition assay

Since remdesivir-TP acts as a substrate of NUDT18, we decided to investigate if remdesivir or its metabolites act as inhibitors of NUDT18 or its close relatives NUDT15 and MTH1. Activity of MTH1 (10 nM) and NUDT15 (10 nM) was tested in assay buffer (0.1 M Tris–acetate pH 7.5, 40 mM NaCl, 1 mM DTT, and 10 mM $Mg(Ac)_2$) fortified with PPase (0.2 U/ml), with 100 μM dGTP in the presence of 1% dimethyl sulfoxide or with 100 μM of remdesivir-TP (#G167050, Biosynth Carbosynth), remdesivir (#AG170167, Biosynth Carbosynth), or remdesivir metabolite (#AG167808, Biosynth Carbosynth). NUDT18 activity was assayed using 100 nM NUDT18 and 100 μM 8-oxo-dGDP in assay buffer. The reaction mixture was incubated for 30 min at 22 °C after which formed Pi was detected by addition of malachite green reagent followed by absorbance measurements at 630 nm in a Hidex spectrophotometer.

Data availability

All data are available from the authors upon request.

Supporting information—This article contains supporting information.

Acknowledgments—The authors thank the Protein Science Facility at Karolinska Institutet/SciLifeLab (http://ki.se/psf) for protein production, Mari Kullman Magnusson for excellent laboratory support, and Louise Sjöholm and Athina Pliakou for administrative support. We thank Dr Maeve Long for linguistic corrections.

Author contributions—A.-S. J., E. R. S., E. H., and M. M. writing–original draft; A.-S. J., E. H., and M. M. conceptualization; A.-S. J., E. R. S., and E. H. methodology; A.-S. J., E. R. S., and E. H. investigation; A.-S. J., E. R. S., and E. H. formal analysis; P. S., T. H., and M. M. supervision; A.-S. J., E. R. S., E. H., M. M., P. S., T. H., and M. M. writing–review and editing; A.-S J and M. M. visualization; A.-S. J., P. S., T. H., and M. M. funding acquisition; A. S. J. validation.

Funding and additional information—This work was supported by the European Research Council, European Union (TAROX Program, ERC-695376 to T. H.), the Swedish Research Council, Sweden (2015-00162, 2017-06095 to T. H. and 2018-03406 to P. S.), the Torsten and Ragnar Söderberg Foundation, Sweden (to T. H.), the Knut and Alice Wallenberg Foundation, Sweden (KAW2014.0273 to T. H.), the Swedish Cancer Society, Sweden (CAN2018/0658 to T. H. and 20 1287 PjF to P. S.), KI funds (2020-02211 to A. S. J), the

Alfred Österlund foundation, Sweden (to P. S.), the Åke Olsson foundation for hematological research (2020-00306 to M. M.). This project has received funding from the Innovative Medicines Initiative 2 Joint Undertaking (JU) under grant agreement No 875510. The JU receives support from the European Union's Horizon 2020 research and innovation programme and EFPIA and Ontario Institute for Cancer Research, Royal Institution for the Advancement of Learning McGill University, Kungliga Tekniska Hoegskolan, Diamond Light Source Limited. This communication reflects the views of the authors and the JU is not liable for any use that may be made of the information contained herein. Funding for open access charge: The Swedish Research Council.

Conflict of interest—The authors declare that they have no conflicts of interest with the contents of this article.

Abbreviations—The abbreviations used are: ITPase, inosine triphosphate pyrophosphatase; MTH1, MutT Homolog 1; NUDT, Nudix hydrolase; PPase, pyrophosphatase.

References

1. de Wit, E., Feldmann, F., Cronin, J., Jordan, R., Okumura, A., Thomas, T., *et al.* (2020) Prophylactic and therapeutic remdesivir (GS-5734) treatment in the rhesus macaque model of MERS-CoV infection. *Proc. Natl. Acad. Sci. U. S. A.* **117**, 6771–6776
2. Beigel, J. H., Tomashek, K. M., Dodd, L. E., Mehta, A. K., Zingman, B. S., Kalil, A. C., *et al.* (2020) Remdesivir for the treatment of Covid-19 - final report. *N. Engl. J. Med.* **383**, 1813–1826
3. Ngo, B. T., Marik, P., Kory, P., Shapiro, L., Thomadsen, R., Iglesias, J., *et al.* (2021) The time to offer treatments for COVID-19. *Expert Opin. Invest. Drugs* **30**, 505–518
4. Artese, A., Svicher, V., Costa, G., Salpini, R., Di Maio, V. C., Alkhatib, M., *et al.* (2020) Current status of antivirals and druggable targets of SARS CoV-2 and other human pathogenic coronaviruses. *Drug Resist. Updat.* **53**, 100721
5. Grein, J., Ohmagari, N., Shin, D., Diaz, G., Asperges, E., Castagna, A., *et al.* (2020) Compassionate use of remdesivir for patients with severe Covid-19. *N. Engl. J. Med.* **382**, 2327–2336
6. Teoh, S. L., Lim, Y. H., Lai, N. M., and Lee, S. W. H. (2020) Directly acting antivirals for COVID-19: where do we stand? *Front. Microbiol.* **11**, 1857
7. Agostini, M. L., Andres, E. L., Sims, A. C., Graham, R. L., Sheahan, T. P., Lu, X. T., *et al.* (2018) Coronavirus susceptibility to the antiviral remdesivir (GS-5734) is mediated by the viral polymerase and the Proofreading exoribonuclease. *mBio* **9**, e00221-18
8. Gordon, C. J., Tchesnokov, E. P., Feng, J. Y., Porter, D. P., and Gotte, M. (2020) The antiviral compound remdesivir potently inhibits RNA-dependent RNA polymerase from Middle East respiratory syndrome coronavirus. *J. Biol. Chem.* **295**, 4773–4779
9. Fischer, W., Eron, J., Holman, W., Cohen, M. S., Fang, L., Szewczyk, L. J., *et al.* (2021) Molnupiravir, an oral antiviral treatment for COVID-19. *medRxiv*. https://doi.org/10.1101/2021.06.17.21258639
10. Bernal, A. J., Gomes da Silva, M. M., Musungaie, D. B., Kovalchuk, E., Gonzalez, A., Delos Reyes, V., *et al.* (2022) Molnupiravir for oral treatment of Covid-19 in nonhospitalized patients. *New Engl. J. Med.* **386**, 509–520
11. Toots, M., Yoon, J. J., Hart, M., Natchus, M. G., Painter, G. R., and Plemper, R. K. (2020) Quantitative efficacy paradigms of the influenza clinical drug candidate EIDD-2801 in the ferret model. *Transl. Res.* **218**, 16–28
12. Sheahan, T. P., Sims, A. C., Zhou, S., Graham, R. L., Pruijssers, A. J., Agostini, M. L., *et al.* (2020) An orally bioavailable broad-spectrum antiviral inhibits SARS-CoV-2 in human airway epithelial cell cultures and multiple coronaviruses in mice. *Sci. Transl. Med.* **12**, eabb5883
13. Painter, G. R., Bowen, R. A., Bluemling, G. R., DeBergh, J., Edpuganti, V., Gruddanti, P. R., *et al.* (2019) The prophylactic and therapeutic activity of a broadly active ribonucleoside analog in a murine model of intranasal venezuelan equine encephalitis virus infection. *Antivir. Res.* **171**, 104597
14. Kabinger, F., Stiller, C., Schmitzoval, J., Dienemann, C., Kokic, G., Hillen, H. S., *et al.* (2021) Mechanism of molnupiravir-induced SARS-CoV-2 mutagenesis. *Nat. Struct. Mol. Biol.* **28**, 740. -+
15. Sidwell, R. W., Huffman, J. H., Khare, G. P., Allen, L. B., Witkowski, J. T., and Robins, R. K. (1972) Broad-spectrum antiviral activity of virazole: 1-beta-D-ribofuranosyl-1,2,4-triazole-3-carboxamide. *Science* **177**, 705–706
16. Reichard, O., Norkrans, G., Fryden, A., Braconier, J. H., Sonnerborg, A., and Weiland, O. (1998) Randomised, double-blind, placebo-controlled trial of interferon alpha-2b with and without ribavirin for chronic hepatitis C. The Swedish Study Group. *Lancet* **351**, 83–87
17. Debing, Y., Jochmans, D., and Neyts, J. (2013) Intervention strategies for emerging viruses: use of antivirals. *Curr. Opin. Virol.* **3**, 217–224
18. Ascioglu, S., Leblebicioglu, H., Vahaboglu, H., and Chan, K. A. (2011) Ribavirin for patients with crimean-Congo haemorrhagic fever: a systematic review and meta-analysis. *J. Antimicrob. Chemother.* **66**, 1215–1222
19. Dokuzoguz, B., Celikbas, A. K., Gok, S. E., Baykam, N., Eroglu, M. N., and Ergonul, O. (2013) Severity scoring index for crimean-Congo hemorrhagic fever and the impact of ribavirin and corticosteroids on fatality. *Clin. Infect. Dis.* **57**, 1270–1274
20. Kamar, N., Izopet, J., Tripon, S., Bismuth, M., Hillaire, S., Dumortier, J., *et al.* (2014) Ribavirin for chronic hepatitis E virus infection in transplant recipients. *New Engl. J. Med.* **370**, 1111–1120
21. Morgenstern, B., Michaelis, M., Baer, P. C., Doerr, H. W., and Cinatl, J. (2005) Ribavirin and interferon-beta synergistically inhibit SARS-associated coronavirus replication in animal and human cell lines. *Biochem. Biophys Res. Commun.* **326**, 905–908
22. Nystrom, K., Wanrooij, P. H., Waldenstrom, J., Adamek, L., Brunet, S., Said, J., *et al.* (2018) Inosine triphosphate Pyrophosphatase dephosphorylates ribavirin triphosphate and reduced enzymatic activity Potentiates mutagenesis in hepatitis C virus. *J. Virol.* **92**, e01087-18
23. Fellay, J., Thompson, A. J., Ge, D., Gumbs, C. E., Urban, T. J., Shianna, K. V., *et al.* (2010) ITPA gene variants protect against anaemia in patients treated for chronic hepatitis C. *Nature* **464**, 405–408
24. Jemth, A. S., Gustafsson, R., Brautigam, L., Henriksson, L., Vallin, K. S. A., Sarno, A., *et al.* (2018) MutT homologue 1 (MTH1) catalyzes the hydrolysis of mutagenic O6-methyl-dGTP. *Nucl. Acids Res.* **46**, 10888–10904
25. Scaletti, E. R., Vallin, K. S., Brautigam, L., Sarno, A., Warpman Berglund, U., Helleday, T., *et al.* (2020) MutT homologue 1 (MTH1) removes N6-methyl-dATP from the dNTP pool. *J. Biol. Chem.* **295**, 4761–4772
26. Valerie, N. C., Hagenkort, A., Page, B. D., Masuyer, G., Rehling, D., Carter, M., *et al.* (2016) NUDT15 hydrolyzes 6-thio-DeoxyGTP to mediate the anticancer efficacy of 6-thioguanine. *Cancer Res.* **76**, 5501–5511
27. Zhang, S. M., Rehling, D., Jemth, A. S., Throup, A., Landazuri, N., Almlof, I., *et al.* (2021) NUDT15-mediated hydrolysis limits the efficacy of anti-HCMV drug ganciclovir. *Cell Chem. Biol.* **28**, 1693–1702. e6
28. Takagi, Y., Setoyama, D., Ito, R., Kamiya, H., Yamagata, Y., and Sekiguchi, M. (2012) Human MTH3 (NUDT18) protein hydrolyzes oxidized forms of guanosine and deoxyguanosine diphosphates: comparison with MTH1 and MTH2. *J. Biol. Chem.* **287**, 21541–21549
29. Hashiguchi, K., Hayashi, M., Sekiguchi, M., and Umezu, K. (2018) The roles of human MTH1, MTH2 and MTH3 proteins in maintaining genome stability under oxidative stress. *Mutat. Res.* **808**, 10–19
30. Carreras-Puigvert, J., Zitnik, M., Jemth, A.-S., Carter, M., Unterlass, J. E., Hallström, B., *et al.* (2017) A comprehensive structural, biochemical and biological profiling of the human NUDIX hydrolase family. *Nat. Commun.* **8**, 1–17
31. Ting Wang, J. F., Schwartz, Karen, Fan, Peidong, Ports, Michael O., Kashishian, Adam, Notte, Gregory T., *et al.* (2020) Direct measurement of the intracellular concentration of 8-oxo-2'-deoxyguanosine-5'-triphosphate by LC-MS/MS. *J. Bioanal. Biomed.* https://doi.org/10.37421/Jbabm.2020.12.237

32. Tempestilli, M., Caputi, P., Avataneo, V., Notari, S., Forini, O., Scorzolini, L., *et al.* (2020) Pharmacokinetics of remdesivir and GS-441524 in two critically ill patients who recovered from COVID-19. *J. Antimicrob. Chemoth.* **75**, 2977–2980
33. Humeniuk, R., Mathias, A., Cao, H., Osinusi, A., Shen, G., Chng, E., *et al.* (2020) Safety, tolerability, and Pharmacokinetics of remdesivir, an antiviral for treatment of COVID-19, in healthy subjects. *Clin. Transl. Sci.* **13**, 896–906
34. Michel, M., Homan, E. J., Wiita, E., Pedersen, K., Almlof, I., Gustavsson, A. L., *et al.* (2020) In silico Druggability assessment of the NUDIX hydrolase protein family as a workflow for target Prioritization. *Front. Chem.* **8**, 443
35. Gad, H., Koolmeister, T., Jemth, A. S., Eshtad, S., Jacques, S. A., Strom, C. E., *et al.* (2014) MTH1 inhibition eradicates cancer by preventing sanitation of the dNTP pool. *Nature* **508**, 215–221
36. Zhang, S. M., Desroses, M., Hagenkort, A., Valerie, N. C. K., Rehling, D., Carter, M., *et al.* (2020) Development of a chemical probe against NUDT15. *Nat. Chem. Biol.* **16**, 1120–1128
37. Loving, K. A. (2014) Structure-based druggability assessment of the mammalian structural proteome with inclusion of light protein flexibility. *PLoS Comput. Biol.* **10**, e1003741
38. Holm, L., and Rosenstrom, P. (2010) Dali server: conservation mapping in 3D. *Nucl. Acids Res.* **38**, W545–W549
39. Waz, S., Nakamura, T., Hirata, K., Koga-Ogawa, Y., Chirifu, M., Arimori, T., *et al.* (2017) Structural and kinetic studies of the human Nudix hydrolase MTH1 reveal the mechanism for its broad substrate specificity. *J. Biol. Chem.* **292**, 2785–2794
40. Baykov, A. A., Evtushenko, O. A., and Avaeva, S. M. (1988) A malachite green procedure for orthophosphate determination and its use in alkaline phosphatase-based enzyme immunoassay. *Anal. Biochem.* **171**, 266–270
41. Sherman, W., Day, T., Jacobson, M. P., Friesner, R. A., and Farid, R. (2006) Novel procedure for modeling ligand/receptor induced fit effects. *J. Med. Chem.* **49**, 534–553